nature electronics

ARTICLES

https://doi.org/10.1038/s41928-021-00655-0

Check for updates

Direct electrical modulation of second-order optical susceptibility via phase transitions

Ying Wang[1,2], Jun Xiao[1], Ting-Fung Chung[1], Zhaoyu Nie[1], Sui Yang[1] and Xiang Zhang[3]✉

Electrical modulation of nonlinear optical signals is crucial for emerging applications in communications and photonic circuits. However, current methods of modulating the second-order optical susceptibility involve indirectly and inefficiently changing the third-order susceptibility. Here we show that electrical switching of the crystal structure of monolayer molybdenum ditelluride can be used to directly modulate the second-order susceptibility. This approach leads to modulation of the second-harmonic generation with an on/off ratio of 1,000 and modulation strength of 30,000% per volt, as well as broadband operation of 300 nm. We also show that molybdenum ditelluride bilayers exhibit opposite modulation trends due to electrically induced heterostructures.

Nonlinear optical properties of crystals are critical for many light–matter interactions including spontaneous parametric downconversion, harmonic generation and four-wave mixing. Dynamic control of nonlinear optical properties is also important in the development of novel photonic applications[1,2], including advanced laser spectroscopy[3], on-demand quantum light sources[4] and photonic logic devices for high-speed photonic computation and storage[5]. Electrical modulation of the second-order nonlinearity $\chi^{(2)}$—through which optical fields interact with a nonlinear medium to produce optical fields with doubled frequency—is especially critical for on-chip applications such as compact lasers and photonic neural networks[6].

Directly modulating $\chi^{(2)}$, however, requires switching the symmetry of a crystal's atomic structure. Structural change in bulk crystals may lead to modulation of the second-harmonic generation (SHG), but it typically requires high temperature or irreversible chemical substitution that are difficult for on-chip device applications. Instead, electric-field-induced second-harmonic (EFISH) generation[7] has been primarily used, which indirectly produces a second-order response through electrical modulation of third-order nonlinear susceptibility $\chi^{(3)}$ under an applied external field (E), that is, $\Delta\chi^{(2)}=\chi^{(3)}E$. The direct-current field redistributes the electrons' wavefunctions and slightly breaks the inversion symmetry, whereas the atomic structure of the crystal remains unchanged. However, being a third-order nonlinearity means the effect is weak and a large operating voltage (up to 100 V) is required for proper modulation. Plasmonics and metamaterials can increase this effect through resonance-induced field enhancement[1,8], but this could limit the wavelength bandwidth to as narrow as 10 nm.

Atomically thin layered materials are promising candidates for nonlinear optical modulation due to their large inherent optical nonlinearities and structural tunability by electrical manipulation. Broken inversion symmetry in monolayer transition metal dichalcogenides (TMDs) results in large second-order susceptibilities, as high as tens of nanometres per volt, which are essential for SHG modulation[9–11]. TMDs also exhibit numerous crystal phases—different intralayer or interlayer atomic arrangements—with distinct crystal symmetries[12]. Being only a few atoms thick also reduces the electrostatic screening effect[13,14] and allows for a large doping population (up to 10^{15} cm^{-2}). Large modifications of electrical properties, such as superconductivity and excitonic states, have been observed in TMDs[15,16]. Electrically controlled phase change in atomically thin crystals has been demonstrated[17,18], and it is possible to explore the electrical modulation of intrinsic $\chi^{(2)}$ through changes in the atomic structure, without the screening effects or high-temperature trigger that make structural changes in bulk materials challenging.

In this Article, we show that the electrical switching of the crystal structure of monolayer molybdenum ditelluride ($MoTe_2$) between non-centrosymmetric and centrosymmetric phases can be used to directly modulate $\chi^{(2)}$. The direct switching of inversion symmetry leads to tunability of the SHG intensity, with an on/off ratio of up to 1,000 and—compared with other leading approaches[19–21]—a two orders of magnitude higher modulation strength of around 30,000% per volt in addition to broadband tunability over a wavelength range of 300 nm. The modulator can robustly operate at room temperature, showing identical hysteresis and on/off ratios after 30 cycles. We also show that a modulator made using bilayer $MoTe_2$ exhibits a reversed gate dependence in SHG modulation due to broken inversion symmetry in the bilayer.

Platform for SHG modulation based on structural change

Figure 1a shows the platform schematics for SHG modulation (Methods provides the fabrication details). Hexagonal $MoTe_2$ flakes (1H and 2H denote monolayer and bilayer flakes, respectively) were mechanically exfoliated onto silicon oxide substrates and grounded by electrodes. An ionic liquid *N*,*N*-diethyl-*N*-(2-methoxyethyl)-*N*-methylammonium bis(trifluoromethylsulfonyl-imide)(DEME–TFSI) is used as the dielectric gate material on top[22], which can provide a large population of carriers (up to 10^{14} cm^{-2}) and possibly trigger the transition from 1H to another lattice configuration, namely, 1T'. We confirm—by Raman spectroscopy—that injecting (withdrawing) carriers into (from) monolayer $MoTe_2$ induces structural transformation between the hexagonal and monoclinic phase (Fig. 1b), which shows consistent Raman frequency changes as reported in a previous study[18]. At 0 V (little carrier doping), two characteristic phonon vibrations of the 1H phase were observed as

[1]Nanoscale Science and Engineering Center (NSEC), University of California at Berkeley, Berkeley, CA, USA. [2]Department of Electrical and Computer Engineering, University of Wisconsin–Madison, Madison, WI, USA. [3]Faculty of Science and Faculty of Engineering, The University of Hong Kong, Hong Kong, China. ✉e-mail: president@hku.edu

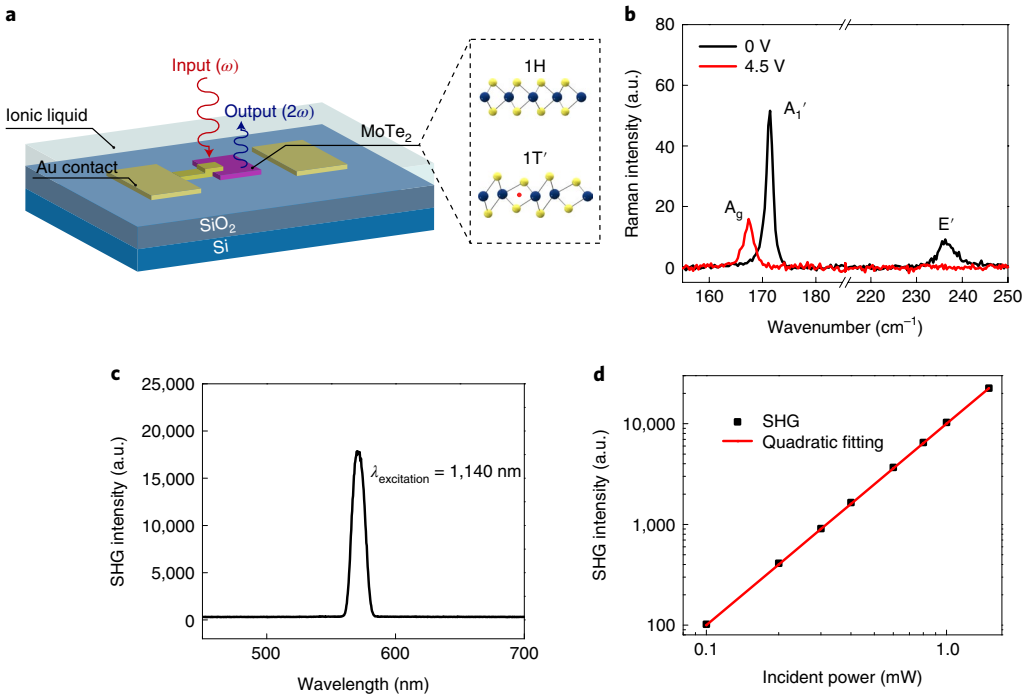

Fig. 1 | Direct electrical modulation of second-order optical susceptibility $\chi^{(2)}$ based on layered $MoTe_2$. **a**, Schematic of an SHG modulator. DEME-TFSI (ionic liquid) can provide electrostatic doping under gate bias (V_g) to drive structural transition between the 1H and 1T' phases in monolayer $MoTe_2$. Side views of the crystal structures of the 1H and 1T' phases of monolayer $MoTe_2$ are shown in the inset. Blue and yellow spheres represent molybdenum and tellurium atoms, respectively. The inversion centre (red dot) is present in 1T′, whereas it is lacking in the 1H phase, making broadband and giant SHG modulation possible through phase transition. **b**, Raman characteristics of 1H ($V_g = 0$ V) and electrically induced 1T' phase ($V_g = 4.5$ V) show distinct vibration modes, confirming the occurrence of a structural phase transition. **c**, Strong SHG from a pristine 1H-$MoTe_2$ without inversion symmetry, under excitation light with 1,140 nm wavelength ($\lambda_{excitation} = 1{,}140$ nm) . **d**, Power dependence of SHG intensity shows an expected quadratic behaviour for such a second-order nonlinear process.

the A_1' mode (at 171.5 cm^{-1}) and E' mode (at 236.0 cm^{-1}). However, at 4.5 V (carrier density, $>2\times10^{14}$ cm^{-2}), the sample exhibits distinct Raman features with only a single peak as the A_g mode at 167.5 cm^{-1}. The emergence of this A_g mode and the disappearance of A_1' and E' modes indicate the formation of the 1T' phase. Such electrically controlled phase transition is robust and reversible as—when the carrier doping is retracted—two phonon modes of the 1H phase (A_1' mode and E' mode) are fully recovered (Supplementary Fig. 1). On the other hand, notable SHG was observed in the 1H phase without inversion symmetry (Fig. 1c). Further, SHG intensity showing a quadratic dependence of the fundamental pump intensity confirms its second-order nonlinear nature (Fig. 1d). In contrast, the monolayer of the 1T' phase has a centrosymmetric centre (marked as a red dot in its lattice structure; Fig. 1a), which is expected to fundamentally eliminate the generation of SHG. The reconfigurable phases of atomically thin layers of $MoTe_2$ are, therefore, a promising route for showing SHG tunability due to the symmetry transition embedded in its structural phase transformation, which dominates the change in nonlinearity.

SHG tunability and modulation strength

To comprehensively characterize SHG tunability associated with the phase transition, we conducted gate-dependent SHG intensity measurements over a broad scan of excitation wavelengths (1,000–1,300 nm). The SHG measurement setup is shown in Supplementary Fig. 2. First, we measured the spectrum of hexagonal monolayer $MoTe_2$ excited at various wavelengths without gate bias. For each discrete excitation, a clear double-frequency peak was observed. Although maintaining the same input power for each excitation, the detected SHG intensity exhibits excitation wavelength dependence for the pristine monolayer (Fig. 2a). The SHG intensity peaks at 570 nm, whereas the signal decreases as it deviates from the centre. This is due to the fact that the corresponding 1,140 nm excitation is resonant with the A exciton in monolayer $MoTe_2$ (ref. [23]), leading to the largest observed SHG intensity. The phase transition of monolayer $MoTe_2$ can be further electrically modulated to control the SHG signals. Before the structural phase transition occurs, the filling of additional carriers simply modifies the electrostatic screening and related excitonic resonance profile. Such a pure electronic effect results in notable intensity change at excitonic resonance pumping, whereas negligible intensity variation is observed at non-resonance excitation. Nevertheless, the maximum relative intensity modulation is less than two times over the whole measurement wavelength range before the structural phase transition takes place (from red to orange curves; Fig. 2b). Further increasing the gate bias beyond 2.9 V (corresponding to a carrier density of ~10^{14} cm^{-2})[17,18], the hexagonal crystal starts to reconfigure into the monoclinic phase. Raman spectra displaying the structural evolution are shown in Supplementary Fig. 3. Accompanying such structural transition, the SHG intensity undergoes a decrease of more than two orders of magnitude for all the wavelengths (Fig. 2b). This leads to strong broadband SHG on/off ratio of up to 1,000. We attribute such large, wavelength-dependent SHG modulation during the phase transition to two factors: the restoration of crystal inversion symmetry and the structure evolution of the electronic band involving the disappearance of excitonic resonance towards the new metallic phase (1T'). The former is expected to be dominant over all the excitation wavelengths, whereas the latter only becomes visible for excitation close to the initial excitonic resonance of the 1H phase.

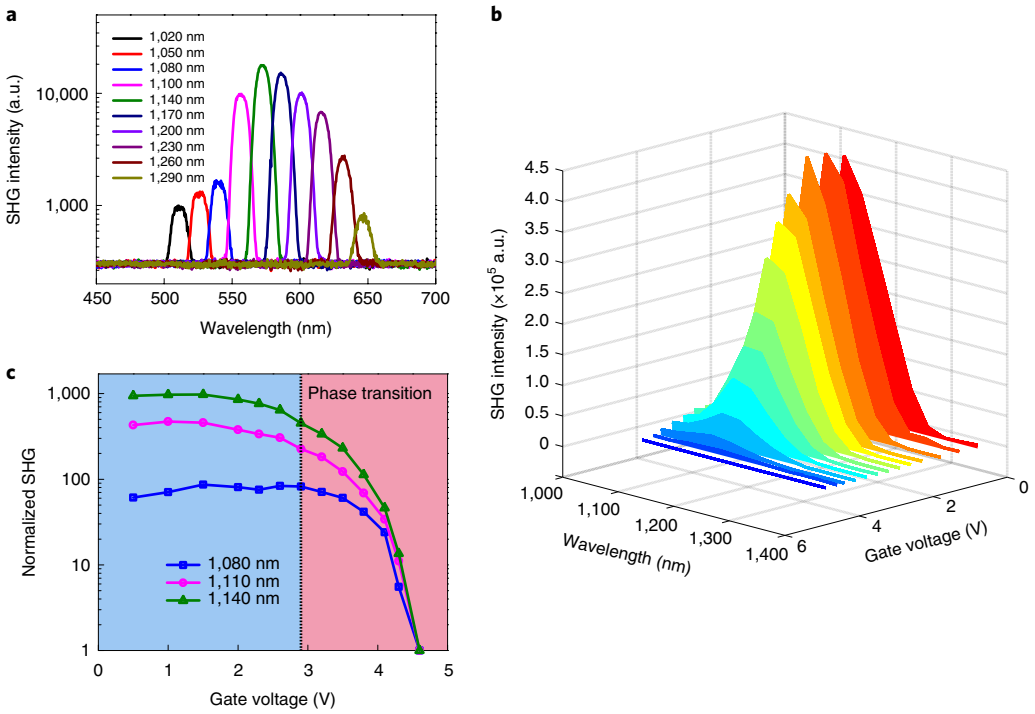

Fig. 2 | Broadband and giant SHG tunability in monolayer $MoTe_2$ through electrically induced phase transition. a, SHG intensity of pristine 1H phase exhibits strong wavelength dependence with a peak resonating with the excitonic resonance. The laser excitation wavelength was scanned from 1,000 nm to 1,290 nm with a fixed input power. **b**, Observation of a decrease in broadband SHG intensity induced by the structural phase transition, which occurs beyond a certain critical gate bias. **c**, Gate-dependent SHG intensity at selective on-resonance and off-resonance excitations. Gate dependence of SHG at off-resonance excitation (1,080 nm) reflects the restoration of inversion symmetry towards the 1T' phase. When the gate bias increases beyond 2.9 V, the SHG intensity shows a sharp decrease of about 100 times, representing a transition from the 1H to 1T' phase. On the other hand, the modulation trend of on-resonance excitation (1,110 nm or 1,140 nm) additionally includes the disappearance of excitonic resonance during phase transition, which gives a modulation depth as large as 1,000 times.

To quantify each contribution, we plot the gate-dependent SHG change under select excitation wavelengths (Fig. 2c), which are at on-excitonic resonance and off-excitonic resonance of the pristine 1H phase. These plots are extracted by linecuts in Fig. 2b. The gate-dependent intensity change under off-resonant excitation at 1,080 nm can exclusively reflect the influence of the restoration of inversion symmetry during transition towards the 1T' phase. This shows that SHG starts to decrease at 2.9 V, indicated by the dashed line and referring to the starting point of the phase transition. Above this critical voltage, SHG steeply decreases, resulting in an intensity on/off ratio of about 100. On the other hand, the change in SHG under resonant excitations induced by a laser at 1,110 and 1,140 nm not only follows the same decreasing trend but also includes the disappearance of excitonic resonance during the phase transition. Thus, a better SHG contrast of 700 times was observed, where the additional sevenfold enhancement is attributed to the disappearance of excitonic resonance. If counting SHG change over the full tuning voltage range, a total SHG on/off ratio can be as large as 1,000, about two orders of magnitude higher than that achieved through excitonic tuning in a previous work[21]. The above findings demonstrate that the large tunability of SHG (up to an on/off ratio of 1,000) is accessible for broadband excitation from 1,000 to 1,380 nm—the accessible wavelengths of the experimental setup. An additional experiment (Supplementary Fig. 4) shows that the working wavelength can be decreased to 800 nm, above the bandgap of the 1H phase, allowing similar tunability. We also estimate $\chi^{(2)} \approx 27\,\mathrm{nm\,V^{-1}}$ for pristine 1H-$MoTe_2$ excited at 1,140 nm; combining the large tunability (a difference of 1,000 times in SHG intensity), $\chi^{(2)}$ accordingly changes by ~33 times (Supplementary Information).

We analysed the electrical modulation strength of SHG[19], which is defined as a relative intensity change in percentage per applied voltage $(\mathrm{SHG_{max}} - \mathrm{SHG_{min}})/(\mathrm{SHG_{min}} \times \Delta V) \times 100\%$. This quantity reflects how efficiently the SHG coefficient can be electrically modulated, which is the key figure of merit for an electrical SHG modulator. During the full sweeping of gate bias, the modification of SHG involves two stages: without and with phase transition. The wavelength-dependent modulation strengths of each stage (shown in Fig. 2b) are compared in Fig. 3a. Below the critical voltage (2.9 V) without the occurrence of phase transition, the strength remains low and is less than 100% per volt, regardless of the excitation wavelengths. Such a small value is expected due to the unchanged crystal symmetry. However, when the gate bias goes beyond 2.9 V, the sudden decrease in SHG within a narrow gate-bias range leads to a gigantic strength—as much as 30,000% per volt for the resonant excitation wavelength. This value is two orders of magnitude higher than those reported based on the EFISH generation mechanism[19,20]. Even at non-resonance excitation, the SHG modulation strength during phase transition can be about 4,200% per volt. This extremely high modulation strength primarily results from the structural phase transition involving the restoration of inversion symmetry, whereas a minor contribution from EFISH generation due to vertical electrical field is possible. This is further supported by a control measurement on the 1H MoS_2 monolayer under the same device configuration (Fig. 3b). The change in SHG intensity in monolayer MoS_2 is much smaller with a modulation strength only below 100% per volt and shows no hysteresis (Supplementary Fig. 5), indicating the absence of a phase transition in MoS_2 due to its much higher transition barrier. This finite modulation is attributed to the

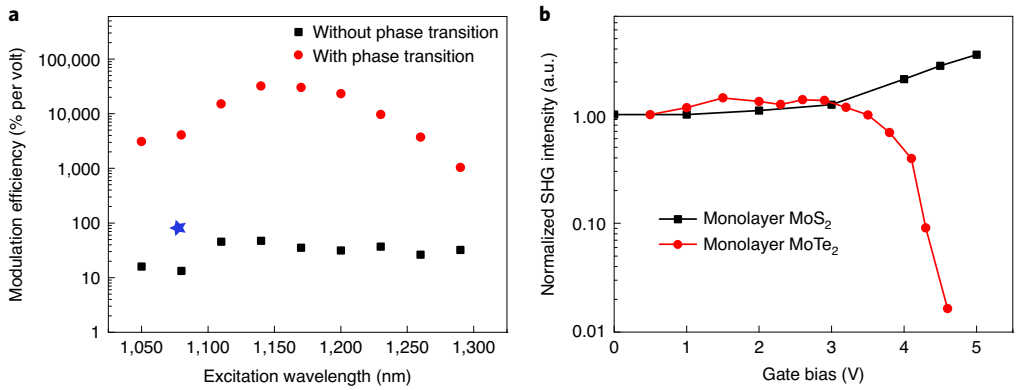

Fig. 3 | Extremely high SHG modulation strength on a monolayer $MoTe_2$ device. As a critical figure of merit for an electrical SHG modulator, the modulation strength is conventionally defined as the relative intensity change in percentage per applied voltage: $(SHG_{max} - SHG_{min})/(SHG_{min} \times \Delta V) \times 100\%$. **a**, Comparison of wavelength-dependent modulation strength with (above 2.9 V) and without (below 2.9 V) phase transition. **b**, Comparison of the gate dependence of SHG intensity in monolayer hexagonal MoS_2 and monolayer $MoTe_2$. Unlike the about two orders of reduction of SHG in $MoTe_2$, it shows an intensity increase of less than five times in monolayer MoS_2 caused by electrically modified oscillation strength or EFISH generation without phase transition. Its corresponding modulation strength is under 100% per volt, marked by the star in **a**. Therefore, electrically induced phase transition involving inversion symmetry change—a novel mechanism—is the key to provide efficient broadband SHG modulation.

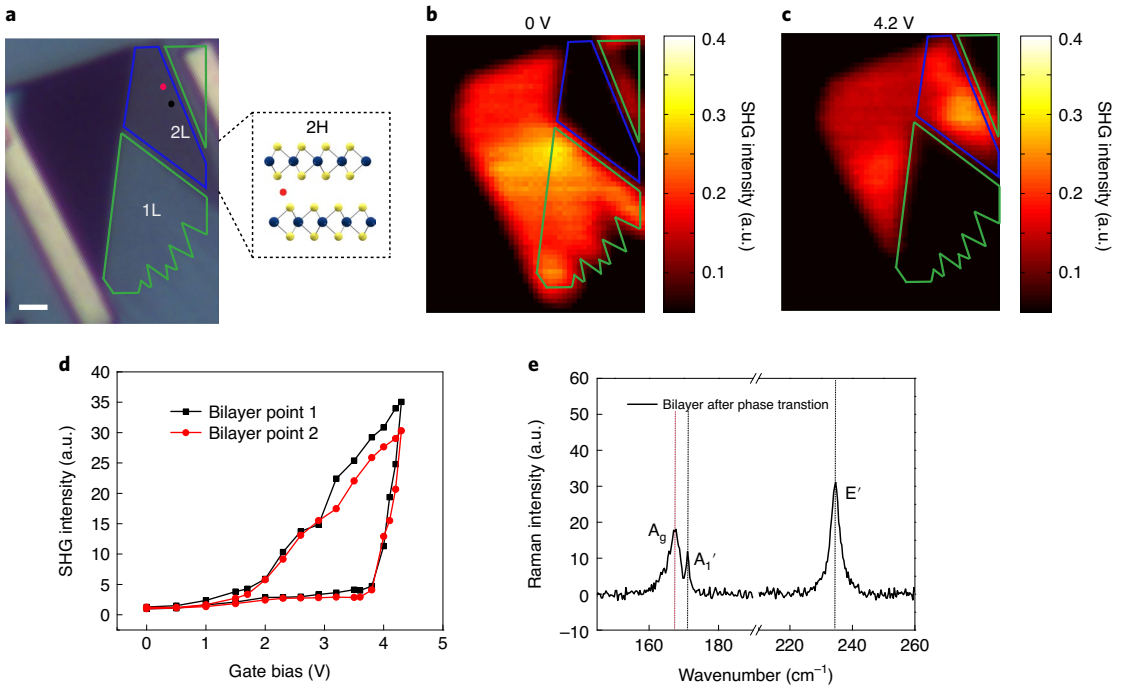

Fig. 4 | Layer-dependent SHG modulation and electrically induced 1T′/1H heterostructures. a, Optical image of the device includes a mixture flake with both monolayer (1L) and bilayer (2L) (enclosed by green and blue lines, respectively), in contact with electrodes represented with yellow rectangles. The scale bar is 5 μm. The side view of the crystal structures of bilayer 2H $MoTe_2$ is shown in the inset. The red dot represents the inversion centre. **b**, At zero bias, the monolayer (1H phase) exhibits strong SHG, whereas the SHG intensity of the bilayer (2H phase) is negligible because of inversion symmetry in even-layer 2H stacking, as shown in **a**. **c**, Reversed layer-dependent spatial distribution of SHG intensity after phase transition at 4.2 V bias. The intensity mapping shows vanishing SHG emission from monolayer $MoTe_2$ whereas substantial SHG intensity from bilayer $MoTe_2$. **d**, Two representative curves of gate-dependent SHG measured in different spatial regions in the bilayer (red and black dots marked in **a**). Unlike the monolayer in which there is a sudden decrease after transitioning into the 1T′ phase, the bilayer shows an opposite trend with a sharp increase when the bias is above 3.8 V, indicating that the initial inversion symmetry has been broken. The excitation wavelength is fixed at 1,060 nm for all the mapping measurements. The observed hysteresis accompanies a structural change in the bilayer region. **e**, Raman spectrum of bilayer $MoTe_2$ at 4.2 V exhibits a double peak at around 170 cm^{-1}, representing the coexistence of hexagonal and monoclinic phases. This suggests the formation of 1T′/1H heterostructure in bilayer $MoTe_2$ through electrostatic doping.

slight electronic absorption profile modified by external doping. Therefore, a sharp phase transition involving inversion-symmetry alternation in our device is the key for achieving ultralarge SHG on/off ratio and extremely high modulation strength. We also verify the robustness of such modulation in a device, where the modulation hysteresis and on/off ratio are identical during 30 cycles at

room temperature (Supplementary Fig. 6). With monolayer hexagonal boron nitride between ionic liquid and $MoTe_2$ (Supplementary Fig. 6), the device is protected from possible electrochemical degradation at high bias. To obtain a clear on/off ratio with our current detection system, the integration time and gate-sweeping time for each gate voltage ranges from 10 ms to 1 s, which means an effective modulation speed for the current device is 1–100 Hz. For future study, such a speed can be potentially boosted into the megahertz region using an ultrathin ionic-liquid gate[24,25].

Electrically induced heterostructure with opposite modulation

We next studied how SHG changes as the layer-dependent inversion symmetry evolves based on the same phase-transition device geometry. For hexagonal lattice with AB stacking, their even-layer crystals preserve the inversion symmetry and forbid SHG[26]. To make a clear comparison between the distinct layers, we mapped out the SHG change on a mixture flake where the monolayer and bilayer coexist (Fig. 4a). Figure 4b,c presents the SHG mapping before (0 V) and after (4.2 V) phase transition under a fixed excitation wavelength of 1,060 nm. At zero voltage (before phase change), SHG is substantial from the monolayer regions but negligible from the bilayer regions, in line with layer-dependent 2H crystal symmetry[10,27]. Whereas at 4.2 V bias, SHG from the monolayer becomes much weaker, and its gate dependence (Supplementary Fig. 7) is consistent with that shown in Fig. 2. Intriguingly, strong SHG was observed from the initially 'dark' bilayer. We summarize the typical gate dependence of SHG (Fig. 4d), extracted from the various positions marked in Fig. 4a. Two stages of SHG evolution were identified. First, a small non-zero SHG for the bilayer increases below 3.8 V, which is suspected from the slight inversion symmetry breaking by the gate bias[28]. Above 3.8 V, a sharp increase occurs and reaches a value comparable to that for the pristine monolayer crystal. Its modulation strength is as good as that in the monolayer but with opposite gate dependence. An intensity hysteresis in the bilayer was observed for a complete gate scan, indicating the emergence of an electrically induced structural change in it.

To clarify the nature of such structural phase transition in the bilayer, we measured the in situ gate-dependent Raman spectrum. Pristine bilayer $MoTe_2$ at zero bias has two characteristic phonon modes: one is at 171.5 cm^{-1} and the other is at 236 cm^{-1} (Supplementary Fig. 8). By increasing the gate bias, we observe the evolution of the Raman spectra in the bilayer, which is notably different from that in the monolayer. Notably, the Raman spectrum of the bilayer with strong SHG at 4.2 V displays two peaks at around 170 cm^{-1} (Fig. 4e). We fitted the Raman mixture with a Lorentz model and obtained two components. One is centred at 167.5 cm^{-1} and the other one remains the same, at 171.5 cm^{-1}, as the original hexagonal phase. The new emergent phonon mode (167.5 cm^{-1}), as a feature of the 1T' phase, suggests this bilayer partially transited into the 1T' phase. Based on both theoretical calculation[29] and experimental demonstration[30], electron doping induced by the ionic liquid mostly concentrates on the very top layer and prevents further doping on the bottom layer through the screening effect. This vertically non-uniform doping distribution gives one order lower carrier doping in the bottom layer, considering a carrier mass of $0.69m_0$ in $MoTe_2$, where m_0 is the electron mass[17,31]. With a doping of ~3.0×10^{14} cm^{-2} at the transition voltage for the bilayer, the doping level in the bottom layer is estimated to be less than 0.4×10^{14} cm^{-2}, which islower than the required doping of ~1.0×10^{14} cm^{-2} for structural transition. Most likely, the 1T' phase can only be formed on the top layer whereas the bottom layer remains in the 1H form. As a result, the strong SHG observed at a high gate bias in bilayer $MoTe_2$ is attributed to both bottom 1H and natural inversion symmetry breaking in such a heterostructure. In this way, our electrical phase-transition device based on an ionic liquid can create a vertical heterostructure in the bilayer and potentially few-layer $MoTe_2$.

Conclusions

We have reported a broadband SHG modulator that uses electrically induced phase changes to manipulate the crystal symmetry of monolayer $MoTe_2$. This approach achieves an SHG on/off ratio of up to 1,000 and modulation strength of 30,000% per volt—two orders of magnitude higher than conventional EFISH generation method—as well as broadband tunability of over 300 nm. Bilayer $MoTe_2$ exhibits the opposite modulation trend due to the structural phase transition selectively occurring at the top layer, enabling a dynamic way to create atomically thin heterostructures. The phase-transition mechanism of $MoTe_2$ has been previously reported[18], but our demonstration of SHG modulation in a device and measurement of its modulation strength, bandwidth, robustness and layer-dependent functionality illustrates the potential of this mechanism in photonic applications. It is also possible that recent progress in obtaining macroscopic flakes[32,33], precise transfer methods[34] and fabricating spatially well-defined high-dielectric gates[35] can accelerate the integration of this SHG modulator into on-chip applications.

Methods

Device fabrication. Atomically thin flakes of $MoTe_2$ were mechanically exfoliated onto a silicon chip covered with a 285-nm-thick thermally grown silicon oxide layer. The thickness of the $MoTe_2$ flakes were first identified by their optical contrast and then verified by Raman frequencies. The typical size of these flakes is in the range of tens of micrometres. After identifying flakes with appropriate thickness, size and shape, we patterned electrodes by standard electron-beam lithography and deposited an electrode metal of indium (5 nm) and gold (100 nm) through thermal evaporation. A drop of ionic liquid (DEME–TFSI) as the electrolyte was cast on top of the device, covering the flakes as well as the metal pad. Before measurement, all the finished devices were annealed at 375 K in a high vacuum (2×10^{-6} torr) for several hours to dehydrate the ionic liquid and to ensure its performance. To avoid electrochemical reaction, measurements on devices without hexagonal boron nitride are done at 220 K and the maximum voltage is limited below 5 V. Devices with a protection layer of monolayer boron nitride are measured at room temperature.

SHG spectroscopy and mapping measurements. The excitation light was extracted using an optical parametric oscillator pumped by a mode-locked titanium–sapphire oscillator. The pulse width of the laser was approximately 200 fs, and the repetition rate was 80 MHz. The excitation laser was linearly polarized and was focused by ×50 near-infrared objective on samples located in a continuous-flow liquid-nitrogen cryostat. The objective is designed with wavelength correction from 400 to 1,800 nm. The SHG signal was detected in the backscattering configuration with broadband short-pass filters and finally collected by a cooled charge-coupled-device spectrometer. By tuning the output wavelength and maintaining the same input power for the optical parametric oscillator, wavelength-dependent SHG can be measured over a large range. The incident fluence is ~500 μJ cm^{-2}. For SHG mapping, the samples are mounted on the same liquid-nitrogen cryostat. A microscope objective (Zeiss ×50; numerical aperture, 0.55) was mounted on a three-dimensional piezostage. The excitation and collection light-spot position in the sample plane was scanned by moving the objective on the piezostage. A sensitive photomultiplier tube was used to analyse the SHG signal in fast mapping.

Raman spectroscopy. Raman spectroscopy was performed using a commercial Raman system (HORIBA LabRAM HR Evolution) under normal incidence of a helium–neon laser (wavelength, 632.8 nm). A continuous-flow liquid-nitrogen cryostat is integrated with this Raman system and measurements are performed under a fixed temperature of ~220 K. A laser beam with a diameter of 1 μm was focused on the samples by ×50 objective.

Data availability

The data that support the findings of this study are available from the corresponding author upon reasonable request.

Received: 11 August 2020; Accepted: 9 September 2021;
Published online: 11 October 2021

References

1. Cai, W., Vasudev, A. P. & Brongersma, M. L. Electrically controlled nonlinear generation of light with plasmonics. *Science* **333**, 1720–1723 (2011).

2. Smith, S. D. Lasers, nonlinear optics and optical computers. *Nature* **316**, 319–324 (1985).
3. Boyd, R. W. & Prato, D. *Nonlinear Optics* (Elsevier Science, 2008).
4. Paesani, S. et al. Generation and sampling of quantum states of light in a silicon chip. *Nat. Phys.* **15**, 925–929 (2019).
5. Caspani, L. et al. Integrated sources of photon quantum states based on nonlinear optics. *Light Sci. Appl.* **6**, e17100 (2017).
6. Woods, D. & Naughton, T. J. Photonic neural networks. *Nat. Phys.* **8**, 257–259 (2012).
7. Terhune, R. W., Maker, P. D. & Savage, C. M. Optical harmonic generation in calcite. *Phys. Rev. Lett.* **8**, 404–406 (1962).
8. Kang, L. et al. Electrifying photonic metamaterials for tunable nonlinear optics. *Nat. Commun.* **5**, 4680 (2014).
9. Kumar, N. et al. Second harmonic microscopy of monolayer MoS_2. *Phys. Rev. B* **87**, 161403 (2013).
10. Song, Y. et al. Second harmonic generation in atomically thin $MoTe_2$. *Adv. Opt. Mater.* **6**, 1701334 (2018).
11. Wen, X., Gong, Z. & Li, D. Nonlinear optics of two-dimensional transition metal dichalcogenides. *InfoMat* **1**, 317–337 (2019).
12. Zhao, M. et al. Atomically phase-matched second-harmonic generation in a 2D crystal. *Light Sci. Appl.* **5**, e16131 (2016).
13. Ye, Z. et al. Probing excitonic dark states in single-layer tungsten disulfide. *Nature* **513**, 214–218 (2014).
14. Chernikov, A. et al. Exciton binding energy and nonhydrogenic Rydberg series in monolayer WS_2. *Phys. Rev. Lett.* **113**, 076802 (2014).
15. Ye, J. T. et al. Superconducting dome in a gate-tuned band insulator. *Science* **338**, 1193–1196 (2012).
16. Chernikov, A., Ruppert, C., Hill, H. M., Rigosi, A. F. & Heinz, T. F. Population inversion and giant bandgap renormalization in atomically thin WS_2 layers. *Nat. Photon.* **9**, 466–470 (2015).
17. Li, Y., Duerloo, K.-A. N., Wauson, K. & Reed, E. J. Structural semiconductor-to-semimetal phase transition in two-dimensional materials induced by electrostatic gating. *Nat. Commun.* **7**, 10671 (2016).
18. Wang, Y. et al. Structural phase transition in monolayer $MoTe_2$ driven by electrostatic doping. *Nature* **550**, 487–491 (2017).
19. Chen, S., Li, K. F., Li, G., Cheah, K. W. & Zhang, S. Gigantic electric-field-induced second harmonic generation from an organic conjugated polymer enhanced by a band-edge effect. *Light Sci. Appl.* **8**, 17 (2019).
20. Ren, M. L., Berger, J. S., Liu, W., Liu, G. & Agarwal, R. Strong modulation of second-harmonic generation with very large contrast in semiconducting CdS via high-field domain. *Nat. Commun.* **9**, 186 (2018).
21. Seyler, K. L. et al. Electrical control of second-harmonic generation in a WSe_2 monolayer transistor. *Nat. Nanotechnol.* **10**, 407–411 (2015).
22. Simon, P. & Gogotsi, Y. Materials for electrochemical capacitors. *Nat. Mater.* **7**, 845–854 (2008).
23. Ruppert, C., Aslan, B. & Heinz, T. F. Optical properties and band gap of single- and few-layer $MoTe_2$ crystals. *Nano Lett.* **14**, 6231–6236 (2014).
24. Liu, A., Gleason, K. K. & Wang, M. Vapor-deposited nanoscale ionic liquid gels as gate insulators for low-voltage high-speed thin film transistors. US patent 10,510,971 (2019).
25. Moon, H. et al. Synthesis of ultrathin polymer insulating layers by initiated chemical vapour deposition for low-power soft electronics. *Nat. Mater.* **14**, 628–635 (2015).
26. Malard, L. M., Alencar, T. V., Barboza, A. P. M., Mak, K. F. & de Paula, A. M. Observation of intense second harmonic generation from MoS_2 atomic crystals. *Phys. Rev. B* **87**, 201401(R) (2013).
27. Li, Y. et al. Probing symmetry properties of few-layer MoS_2 and h-BN by optical second-harmonic generation. *Nano Lett.* **13**, 3329–3333 (2013).
28. Yu, H., Talukdar, D., Xu, W., Khurgin, J. B. & Xiong, Q. Charge-induced second-harmonic generation in bilayer WSe_2. *Nano Lett.* **15**, 5653–5657 (2015).
29. Roldán, R., Cappelluti, E. & Guinea, F. Interactions and superconductivity in heavily doped MoS_2. *Phys. Rev. B* **88**, 054515 (2013).
30. Lu, J. M. et al. Evidence for two-dimensional Ising superconductivity in gated MoS_2. *Science* **350**, 1353–1357 (2015).
31. Ramasubramaniam, A. Large excitonic effects in monolayers of molybdenum and tungsten dichalcogenides. *Phys. Rev. B* **86**, 115409 (2012).
32. Xu, X. et al. Seeded 2D epitaxy of large-area single-crystal films of the van der Waals semiconductor 2H $MoTe_2$. *Science* **372**, 195–200 (2021).
33. Liu, F. et al. Disassembling 2D van der Waals crystals into macroscopic monolayers and reassembling into artificial lattices. *Science* **367**, 903–906 (2020).
34. Shim, J. et al. Controlled crack propagation for atomic precision handling of wafer-scale two-dimensional materials. *Science* **362**, 665–670 (2018).
35. Wang, X. et al. Realization of vertical metal semiconductor heterostructures via solution phase epitaxy. *Nat. Commun.* **9**, 3611 (2018).

Acknowledgements

This work is supported by the Gordon and Betty Moore Foundation (award no. 5722) and the Ernest S. Kuh Endowed Chair Professorship.

Author contributions

Y.W. and X.Z. initiated the research and designed the experiments. Y.W. and J.X. performed the SHG measurements. Y.W. and T.-F.C. fabricated the devices. Y.W. J.X., Z.N. and S.Y. analysed the data with X.Z. All the authors contributed to the writing of the manuscript.

Competing interests

The authors declare no competing interests.

Additional information

Supplementary information The online version contains supplementary material available at https://doi.org/10.1038/s41928-021-00655-0.

Correspondence and requests for materials should be addressed to Xiang Zhang.

Peer review information *Nature Electronics* thanks Ueli Koch, Zheng Liu and Shuang Zhang for their contribution to the peer review of this work.

Reprints and permissions information is available at www.nature.com/reprints.

Publisher's note Springer Nature remains neutral with regard to jurisdictional claims in published maps and institutional affiliations.